

# CONTINUOUS STRUCTURE BASED BAYESIAN COMPRESSIVE SENSING FOR SPARSE RECONSTRUCTION OF TIME-FREQUENCY DISTRIBUTIONS

*Qisong Wu, Yimin D. Zhang, and Moeness G. Amin*

Center for Advanced Communications, Villanova University, Villanova, PA 19085, USA

## ABSTRACT

In this paper, we propose a Bayesian compressive sensing algorithm for effective reconstruction of sparse signals that demonstrate sparsity as continuous but irregular narrow strips in a multi-dimensional space. Among many applications of this class of representations are the two-dimensional time-frequency distributions (TFDs) of radar signals, which are often modeled as frequency modulated (FM) signals characterized by their sparse and continuous instantaneous frequencies. A spike-and-slab prior is introduced to statistically encourage sparsity of the time-frequency representations (TFRs) across each segmented time-frequency region, and a patterned prior is imposed to enforce the continuous structure of the TFR. Compared with the existing sparse signal reconstruction techniques, the proposed technique achieves improved interpretation of the TFD, particularly when the signals are noisy or with missing samples.

**Index Terms**— Time-frequency analysis, Bayesian compressive sensing, missing data sample, continuous structure, sparse reconstruction

## 1. INTRODUCTION

Nonstationary signals, particularly those consisting of a single- or multi-component waveforms with instantaneously narrowband characterizations, arise in a wide class of active and passive sensing modalities, such as radar, sonar, speech, and electromyographic recording. Time-frequency representations (TFRs) enable separation of nonstationary signals that are mixed in both time and frequency domains [1–6]. The simplest and fastest quadratic TFR is the single and multiple-window spectrograms which can be applied to a large class of multi-component nonstationary signals, whereas the most appropriate representation for linear FM signals is the Wigner-Ville distribution (WVD). Due to the power concentrations of nonstationary signals over the joint time-frequency (TF) variables, the signatures of such signals, for most commonly used TFRs, usually occupy sparse but continuous regions in the TF domain [7–10]. For example, frequency-modulated (FM) signals are characterized by continuous instantaneous frequencies and, therefore, have a sparse presence in the TF domain. As such, the recent compressive sensing (CS) and

sparse signal reconstruction techniques [11, 12] can be used for effective TFRs. These reconstruction techniques are not Fourier based and, as such, the resolution obtained does not explicitly depend on the employed data segment length and is not bounded by the Rayleigh limit. Attempts to enhance resolution in the time-frequency domain have so far applied the parametric approach in lieu of Fourier transform [13, 14].

In many real-world applications, nonstationary signals are often observed with missing samples due to fading, obstruction, and/or impulsive noise [10]. Missing data samples would yield spreading artifacts that are distributed in the entire TF domain [8]. Unlike conventional sparse TFR reconstruction techniques that are built upon the two-dimensional (2-D) Fourier relationship between the TF domain and the ambiguity function domain representations [15], the approach proposed in [8] exploits the one-dimensional (1-D) Fourier relationship between the TF domain and the instantaneous auto-correlation function (IAF) domain and, as such, offers two important advantages: (a) It significantly reduces the dimension of the dictionary matrix and, thereby, the complexity of CS reconstructions; (b) It allows the flexible selection of the CS reconstruction over specific time-domain entry and, when using the orthogonal matching pursuit (OMP) [16] or related algorithms, enables specification of the sparsity, i.e., the number of nonzero entries, in each time instant. By separately processing the TFR reconstruction in each time instant, however, this method does not utilize an important information relevant to the continued structure of TF signatures. As such, the approach may generate isolated or sporadic entries in the reconstructed TFR in the presence of missing data and/or measurement noise.

In this paper, inspired by the structure exploitation in the CS techniques [17, 18], a novel Bayesian CS (BCS) approach is proposed for sparse nonstationary signal reconstruction with missing data samples by exploiting the continuous structure of the TF signatures. As such, while it shares similarities with the existing structure exploiting CS techniques, different patterned priors are used in the proposed work. To facilitate the 2-D continuous structures defined in the joint 2-D TF domain, the IAF domain is divided into sections, each consisting of multiple time-domain entries, so that the continuity with neighboring pixels can be utilized to perform sparse TFR reconstruction. The proposed approach not only preserves

the continuous structure of TF signatures, but also effectively suppresses anomalies and isolated signature.

**Notations.** We use lower-case (upper-case) bold characters to denote vectors (matrices).  $\mathcal{F}_x$  and  $\mathcal{F}_x^{-1}$  respectively represent the discrete Fourier Transform (DFT) and inverse DFT (IDFT) with respect to  $x$ . In particular,  $\mathbf{I}_N$  denotes the  $N \times N$  identity matrix.  $(\cdot)^T$  and  $(\cdot)^*$  respectively denote the transpose and complex conjugates of a matrix or vector,  $p(\cdot)$  denotes the probability density function (pdf), and  $\mathcal{CN}(x|a, b)$  implies that random variable  $x$  follows a complex Gaussian distribution with mean  $a$  and variance  $b$ . Furthermore,  $\delta(x)$  is the Dirac delta function of  $x$ , and ‘ $\circ$ ’ denotes element-wise (Hadamard) multiplication.

## 2. TIME-FREQUENCY REPRESENTATION WITH MISSING DATA

### 2.1. Signal Model

Consider a discrete-time signal,  $x(t)$  with  $t \in [1, \dots, T]$ , which may consist of a single or multiple components of FM signals. Denote  $y(t)$  as its observation data with  $N$  missing samples, where  $0 \leq N < T$ . The missing sample positions are assumed to be randomly distributed over time. As such,  $y(t)$  can be regarded as the product of  $x(t)$  and an observation mask  $b(t)$ , i.e.,

$$y(t) = x(t) \cdot b(t), \quad (1)$$

where

$$b(t) = \begin{cases} 1, & \text{if } t \in \mathcal{S}, \\ 0, & \text{if } t \notin \mathcal{S}, \end{cases} \quad (2)$$

with  $\mathcal{S} \subset \{1, \dots, T\}$  is the set of observed time instants and its cardinality is  $|\mathcal{S}| = T - N$ .

### 2.2. Time-Frequency Representation

The discrete IAF of  $x(t)$  is defined as

$$C_{xx}(t, \tau) = x(t + \tau)x^*(t - \tau), \quad (3)$$

with  $\tau$  denoting the time-lag [1, 2, 8]. The IAF of observed data  $y(t)$  can be expressed as

$$C_{yy}(t, \tau) = C_{xx}(t, \tau)C_{bb}(t, \tau), \quad (4)$$

where  $C_{bb}(t, \tau)$  is the IAF of the observation mask  $b(t)$  [8].

The DFT of the IAF with respect to  $\tau$  is the WVD, which denotes the TF characteristics of the signal [1, 2, 8], expressed as

$$W_{xx}(t, f) = \mathcal{F}_\tau[C_{xx}(t, \tau)] = \sum_{\tau} C_{xx}(t, \tau)e^{-j4\pi f\tau}. \quad (5)$$

Note that  $4\pi$  is used in the DFT instead of  $2\pi$  because the actual time-lag in (3) is  $2\tau$ . Similarly, the WVD of the

observed data  $y(t)$  can be represented as,

$$W_{yy}(t, f) = \sum_{\tau \in \mathcal{S}_\tau(t)} C_{yy}(t, \tau)e^{-j4\pi f\tau}, \quad (6)$$

where  $\mathcal{S}_\tau(t)$  is the set of nonzero  $\tau$  entries for a specific  $t$ . The missing data samples lead to spreading artifacts that are randomly distributed in the entire TF domain [8]. According to the analysis in [8], such effect can be mitigated through a proper filter or kernel. One of the best choices for this purpose is the adaptive optimal kernel (AOK) [19]. Sparsity-aware adaptive kernels are also recently developed to better deal with data including missing samples [20].

When the signals, such as FM signals, are sparsely represented in the entire TF domain, their TFR can be reconstructed using the CS technique. For notation convenience, we denote  $\mathbf{c}^{[t]}$  as a vector that consists of all IAF entries along the  $\tau$  dimension corresponding to time  $t$ , and  $\mathbf{w}^{[t]}$  as a vector contains all the TFR entries with respect to the frequency for the same time  $t$ . According to the Fourier relationship between the IAF and the TFR as in Eq. (6), we obtain

$$\mathbf{c}^{[t]} = \Phi \mathbf{w}^{[t]} + \boldsymbol{\epsilon}^{[t]}, \quad t \in [1, \dots, T], \quad (7)$$

where  $\Phi$  is a matrix for the IDFT operation with respect to  $f$ . It should be noted that  $\mathbf{w}^{[t]}$  is a smoothed version of the IAF when a proper kernel is applied.

## 3. CONTINUOUS STRUCTURE BAYESIAN COMPRESSIVE SENSING

A number of inversion algorithms, such as the orthogonal matching pursuit (OMP) [16], basis pursuit [21], and sparse Bayesian learning [22–25], can be used to perform TFR reconstruction. In [8], the OMP algorithm is used to effectively recover the sparse TFR by specifying the number of nonzero entries in each time instant. To exploit the continuous structure of the TFR, however, the BCS-based approaches are considered most capable and convenient due to their flexibility of employing proper priors for this purpose. In the following, we develop a new BCS-based approach for the reconstruction of sparse TFR signatures by exploiting the continuous TFR structure based on a block of IAF results occupying multiple neighboring time instants.

To encourage sparsity of the TF signatures, we place a spike-and-slab prior to  $\mathbf{w}$  [26], i.e.,

$$p\left(w_l^{[t]} \mid \pi_l^{[t]}, \beta_0^{[t]}\right) = \left(1 - \pi_l^{[t]}\right) \delta\left(w_l^{[t]}\right) + \pi_l^{[t]} \mathcal{CN}\left(w_l^{[t]} \mid 0, [\beta_0^{[t]}]^{-1}\right), \quad (8)$$

where  $l \in [1, \dots, T]$  is the frequency domain index. In addition,  $\pi_l^{[t]}$  is the prior probability of a nonzero element, and  $\beta_0^{[t]}$  is the precision (reciprocal of variance) of the complex Gaussian distribution.

To make the inference analytical, we introduce the product of two latent variable  $w_l^{[t]} = z_l^{[t]}\theta_l^{[t]}$  to follow the pdf in Eq. (8), where  $\theta_l^{[t]}$  follows a complex Gaussian distribution  $\mathcal{CN}(\theta_l^{[t]} | 0, [\beta_0^{[t]}]^{-1})$  and  $z_l^{[t]}$  follows the Bernoulli distribution  $\text{Bern}(\pi_l^{[t]})$ .  $z_l^{[t]}$  is a binary variable with  $z_l^{[t]} = 0$  corresponding to zero value for the  $l$ th entry in the time  $t$ . To acquire the tractable posterior of  $\beta_0^{[t]}$ , we place a Gamma prior, which is conjugate to the Gaussian distribution, on  $\beta_0^{[t]}$ , i.e.,  $\beta_0^{[t]} \sim \text{Gamma}(a, b)$ . Without loss of generality, a complex Gaussian prior is placed on the additive noise as  $\epsilon_k^{[t]} \sim \mathcal{CN}(0, \alpha^{-1})$  with  $k \in 1, \dots, K$ . In the similar way, we place a Gamma prior on  $\alpha$  to acquire an analytical posterior distribution, i.e.,  $\alpha \sim \text{Gamma}(a_0, b_0)$ .

To encourage continuity in the joint TF domain, we utilize data in the neighborhood time instants between  $t - D$  and  $t + D$ , when the TF signatures in the time instant  $t$  are estimated. For simplicity,  $D = 1$  is assumed throughout this paper. Based on the idea of continuity, we categorize the relationship into three different patterns, termed as *Pattern 1* (“strong rejection”), *Pattern 2* (“strong acceptance”), and *Pattern 3* (“weak rejection”), respectively. As shown in Fig. 1, we define two variables  $\kappa_l^{[t]} = \sum \tilde{z}_{t_l}$  with  $\tilde{z}_{t_l} = [\tilde{z}_1, \dots, \tilde{z}_6]$  and  $\eta_l^{[t]} = \sum_{i=1}^3 \tilde{z}_i \tilde{z}_{7-i}$ , which respectively represent the number of nonzero neighboring entries and the number of nonzero diagonal pairs.

The three patterns are detailed below. Note that the patterns we used herein differs from those used in [17, 18] in two aspects. First, only the number of nonzero neighboring entries is used in [17, 18] in determining the prior, whereas the diagonal pair is considered more important in this paper. Second, a large prior is placed in [17, 18] when the number of the nonzero neighboring entries is high, whereas in our approach the case with only one pair of the nonzero diagonal entries is most favorable. Note that the vertical pixel pair is excluded in Fig. 1 because these pixels tend to broad the signal bandwidth whereas the underlying FM signals are instantaneously narrowband.

Pattern 1 includes two cases of  $\kappa_l^{[t]} = 0$  or  $\eta_l^{[t]} = 3$ , as shown in Fig. 1(a). In  $\kappa_l^{[t]} = 0$  case, all of neighbors are zero valued, and thus the  $l$ th entry would be zero valued with a high probability. By placing a low value of prior in this case, isolated signatures can be effectively suppress. In  $\eta_l^{[t]} = 3$  case, all the neighbors are nonzero valued. This was the favorable situation in [17, 18] when an extended target is considered, but we consider the  $l$ th entry to take a zero valued with a high probability because the TFR is instantaneously narrowband. Therefore, this strong rejection pattern not only suppresses those isolated signatures, but also effectively prevents the nonzero entries to be broadly extended in frequency domain. In these cases,  $e_0 < f_0$  is assumed in prior  $\text{Beta}(e_0, f_0)$  to encourage a small value of

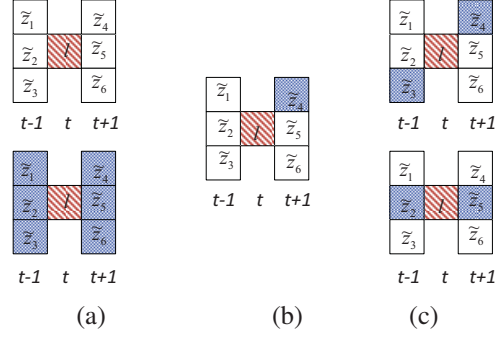


**Fig. 1.** Three pattern for 2-D image. White squares denote entries with zeros amplitudes, blue shaded squares denote the entry with nonzero amplitudes, and red shaded squares denote the entry under test. (a) Pattern 1: strong rejection; (b) Pattern 2: examples for weak rejection with  $\kappa_l^{[t]} = 1$  case; (c) Pattern 3: examples for strong acceptance with  $\eta_l^{[t]} = 1$  case.

$\pi_l^{[t]}$  so as to reject this entry.

Pattern 2 includes those cases of  $\kappa_l^{[t]} > 0$  or  $\eta_l^{[t]} \neq 1$ . Fig. 1(b) shows one of the examples with a single nonzero neighboring entry. In these cases, the probability that the  $l$ th entry takes zero values is fair, and  $e_1 = f_1$  is used in the prior  $\text{Beta}(e_1, f_1)$  to exert non-informative prior on  $\pi_l^{[t]}$ .

Pattern 3 consists of those cases with  $\eta_l^{[t]} = 1$ . Fig. 1(c) show two examples of such cases. We confidently believe that the  $l$ th entry would take a nonzero value with a high probability when nonzero neighboring entries have such continuous and symmetric structure in the 2-D TF domain as instantaneously narrowband FM signals are concerned. In this case,  $e_2 > f_2$  in the prior  $\text{Beta}(e_2, f_2)$  is assumed to encourage a large value of  $\pi_l^{[t]}$  to accept this entry.

## 4. BAYESIAN INFERENCE

We adopt a Gibbs sampler to carry out the Bayesian inference of the proposed algorithm. The posterior distributions of each random variable will be analytically obtained based on the conjugate property.

### 4.1. Updating paired variables $\{\theta^{[t]}, \mathbf{z}^{[t]}\}$

The paired Gibbs sampler iteratively samples from the following conditional pdf,

$$p\left(z_l^{[t]}, \theta_l^{[t]} \mid \theta_{\setminus l}^{[t]}, \mathbf{z}_{\setminus l}^{[t]}, \mathbf{c}^{[t]}\right) = p\left(\theta_l^{[t]} \mid z_l^{[t]}, \theta_{\setminus l}^{[t]}, \mathbf{z}_{\setminus l}^{[t]}, \mathbf{c}^{[t]}\right) \times p\left(z_l^{[t]} \mid \theta_{\setminus l}^{[t]}, \mathbf{z}_{\setminus l}^{[t]}, \mathbf{c}^{[t]}\right), \quad (9)$$

where  $\theta_{\setminus l}^{[t]}$  and  $\mathbf{z}_{\setminus l}^{[t]}$  respectively denote  $\theta_l^{[t]}$  except the variable  $\theta_l^{[t]}$  and  $\mathbf{z}^{[t]}$  except the variable  $z_l^{[t]}$ .

The probability  $p\left(z_l^{[t]} = 1 \mid \boldsymbol{\theta}_{\setminus l}^{[t]}, \mathbf{z}_{\setminus l}^{[t]}, \mathbf{c}^{[t]}\right)$  is acquired analytically as [26]

$$p\left(z_l^{[t]} = 1 \mid \boldsymbol{\theta}_{\setminus l}^{[t]}, \mathbf{z}_{\setminus l}^{[t]}, \mathbf{c}^{[t]}\right) = \frac{\beta_l^{[t]} \mathcal{CN}\left(0, [\beta_l^{[t]}]^{-1}\right)}{1 - \beta_l^{[t]} \mathcal{CN}\left(u_l^{[t]}, \sigma_l^{[t]}\right)}, \quad (10)$$

where  $u$  is derived as

$$u_l^{[t]} = [\sigma_l^{[t]}]^{-1} \alpha \boldsymbol{\phi}_l^H \mathbf{c}^{[t]}, \quad (11)$$

$$\sigma_l^{[t]} = \left(\alpha \boldsymbol{\phi}_l^H \boldsymbol{\phi}_l + \beta_l^{[t]}\right)^{-1}, \quad (12)$$

$\mathbf{c}_{\setminus l}^{[t]} = \mathbf{c}^{[t]} - \sum_{k \neq l} \boldsymbol{\phi}_k z_k^{[t]} \theta_k^{[t]}$ , and  $\boldsymbol{\phi}_l$  represents the  $l$ th column of the measurement matrix  $\Phi$ . The conditional distribution of  $p(\theta_l^{[t]} \mid z_l^{[t]} = 1, \boldsymbol{\theta}_{\setminus l}^{[t]}, \mathbf{z}_{\setminus l}^{[t]}, \mathbf{c}^{[t]})$  can be expressed as

$$p\left(\theta_l^{[t]} \mid z_l^{[t]} = 1, \boldsymbol{\theta}_{\setminus l}^{[t]}, \mathbf{z}_{\setminus l}^{[t]}, \mathbf{c}^{[t]}\right) = \mathcal{CN}\left(\theta_l^{[t]} \mid u_l^{[t]}, \sigma_l^{[t]}\right). \quad (13)$$

For  $z_l^{[t]} = 0$ , because the value of  $\theta_l^{[t]}$  does not affect the result of  $w_l^{[t]}$ , we conveniently draw the value of variable  $\theta_l^{[t]}$  from its prior.

#### 4.2. Updating mixing weight $\pi^{[t]}$

Each element  $\pi_l^{[t]}$  is chosen according to its corresponding sparsity pattern, i.e.,  $\pi_l^{[t]}$  is assigned as  $\pi_{q_l}^{[t]}$  for sparsity pattern  $q \in \{0, 1, 2\}$ . The Beta distribution on  $\pi_{q_l}^{[t]}$  leads to an analytical posterior distribution for a certain sparsity pattern  $q$  as [17],

$$p\left(\pi_{q_l}^{[t]} \mid \mathbf{e}, \mathbf{f}, \mathbf{z}^{[t]}\right) = \text{Beta}(\tilde{e}_q, \tilde{f}_q), \quad (14)$$

where  $\tilde{e}_q = e_q + \kappa_l + z_l^{[t]}$ ,  $\tilde{f}_q = f_q + \nu_l + 1 - \kappa_l - z_l^{[t]}$  with  $l \in \{1, \dots, T\}$ , and  $\nu_l$  is the length of  $\mathbf{z}_{\eta_l}^{[t]}$ .

#### 4.3. Updating signal precision $\beta^{[t]}$

By utilizing the conjugate property of the Gaussian and Gamma distributions, we analytically acquire the posterior distribution of the precision variable  $\beta_l^{[t]}$  as

$$p(\beta_l^{[t]} \mid a, b, \boldsymbol{\theta}^{[t]}) = \text{Gamma}\left(a + \frac{1}{2}, b + \frac{\|\boldsymbol{\theta}_l^{[t]}\|^2}{2}\right). \quad (15)$$

#### 4.4. Updating noise precision $\alpha$

In the similar manner with  $\beta_l$ , we also obtain the posterior distribution of noise precision  $\alpha_l$

$$p(\alpha \mid c, d, \mathbf{c}^{[t]}, \Phi, \boldsymbol{\theta}^{[t]}, \mathbf{z}^{[t]}) = \text{Gamma}(\tilde{a}_0, \tilde{b}_0), \quad (16)$$

where  $\tilde{a}_0 = a_0 + K/2$ , and  $\tilde{b}_0 = \|\mathbf{c}^{[t]} - \Phi(\boldsymbol{\theta}^{[t]} \circ \mathbf{z}^{[t]})\|^2/2$ .

## 5. SIMULATION RESULTS

Two simulation examples are provided in this section. In the first example, a two-component FM signal are used. The instantaneous phases of the two components are respectively expressed as,

$$\phi_1(t) = 0.05t_1 + 0.1t_1^2/T + 0.1t_1^3/T^2, \quad (17)$$

$$\phi_2(t) = 0.15t_2 + 0.1t_2^2/T + 0.1t_2^3/T^2, \quad (18)$$

where  $t_1 \in [1, \dots, 3T/4]$ ,  $t_2 \in [T/4 + 1, \dots, T]$ , and  $T$  is chosen to be 128. The powers of these two FM components are the same and the input signal-to-noise ratio (SNR) of each component is 10 dB. Fig. 2(a) shows the real-part waveform with 50% randomly missing samples, and their corresponding WVD and IAF are shown in Figs. 2(b) and 2(c). We have also included the ambiguity function (AF) in Fig. 2(d) for reference. Consider the fact that the IAF is a product of the original IAF and the IAF of the mask function that nullifies its presence in a large amount of entries, as shown in Fig. 2(b), it would lead to spreading artifacts which are randomly distributed in both the TF and AF domains, as shown in Figs. 2(c) and 2(d).

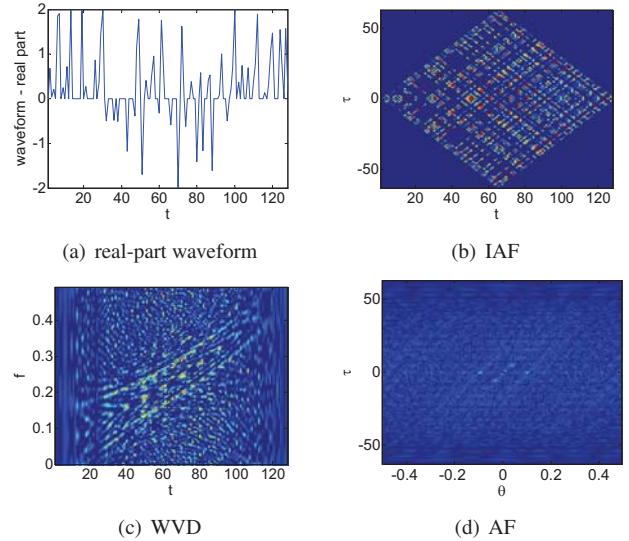


**Fig. 2.** Waveform and transformed domain representations of a two-component FM signal with 50% of missing samples (example 1).

The time-frequency distribution (TFD) obtained from the AOK is shown in Fig. 3(a) for the missing samples. It is evident that the AOK significantly mitigates the missing data artifacts and cross-terms between the two components, while preserving the auto-term characteristics. The resulting TFD shows a clear auto-term characteristics, even with the 50% of missing samples. Similar with the approach proposed

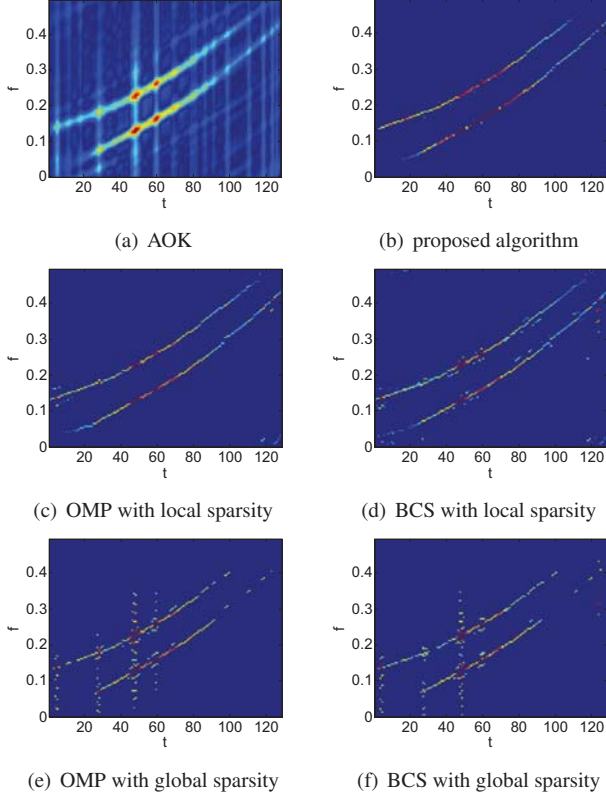


**Fig. 3.** TFD results obtained from different methods (example 1).

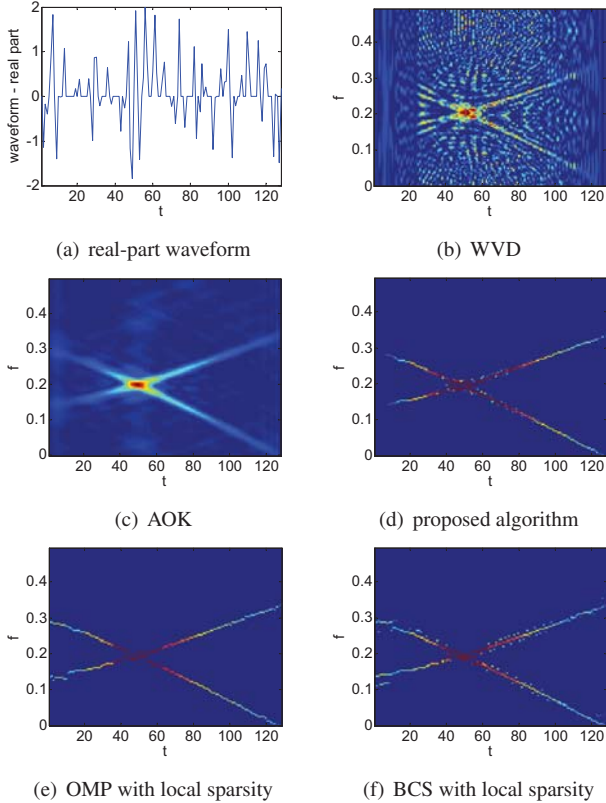


**Fig. 4.** TFD results obtained from different methods (example 2).

in [8], we acquire the TFD by individually performing the OMP algorithm in each time instant assuming a sparsity of 2, and the results are shown in Fig. 3(c). The auto-term signatures are generally reconstructed, but it is observed that the reconstructed TF signatures are discontinuous, and there are some noticeable spurious entries when  $t > 3T/4$  for the signal in Eq. (17) and  $t < T/4$  for signal in Eq. (18), where the true sparsity is 1. By utilizing the same strategy with [8] that separately performs the CS technique in each time, but utilizes the BCS algorithm [22] rather than the OMP, Fig. 3(d) shows the reconstructed result with a few isolated and sporadic TF signatures. Unlike the strategy used in the previous two simulations that take advantage of the local sparsity of TF signatures, we present the results of both OMP and BCS algorithms that use the global sparsity in the entire TF domain, and the results are respectively shown in Fig. 3(e) and 3(f). It is evident that the strategy with the local sparsity has the potential of capturing the TF characteristics and has better performance than that with the global sparsity, particularly when the missing samples are present, because both OMP and BCS would select those signatures with strong powers in the entire TF domain. By enforcing the patterned prior for the structure exploiting Bayesian framework, the proposed algorithm acquires the reconstructed result, as shown in Fig. 3(b). It is clear that the reconstructed TF signatures depicts a continuous structure with isolated or sporadic entries effectively suppressed. The proposed algorithm also has the capability of automatically inferring the sparsity and correctly recovering those signatures.

The second example considers two FM signals whose instantaneous frequencies intersect in the TF domain. The instantaneous phases of the two FM components are expressed as

$$\phi_1(t) = 0.15t + 0.05t^2/T + 0.1t^3/3T^2, \quad (19)$$

$$\phi_2(t) = 0.3t - 0.1t^2/T + 0.1t^3/3T^2, \quad (20)$$

for  $t \in [1, T]$ . Similar to the first example, the input SNR is 10 dB, and 50% samples are missing. The observed waveform is shown in Fig. 4(a), and the corresponding WVD is shown in Fig. 4(b), which is cluttered by the cross-terms as well as the artifacts due to missing data samples. The TFD obtained from the AOK is shown in Fig. 4(c) with significant reduction of the cross-terms and artifacts. The proposed algorithm is used to achieve sparse reconstruction from the kernelled TFD, and the result is shown in Fig. 4(d). It is observed that reconstructed TFD is continuous along time domain through placing the patterned prior to encourage horizontal continuity. While there is some discontinuity around the intersection due to the discouraged pattern, the results are much better than the reconstructed results obtained from the OMP and BCS algorithms, as respectively shown in Figs. 4(e) and 4(f). The latter results show noticeable discontinuity and speckles in other regions.

## 6. CONCLUSION

Compressive sensing (CS) based time-frequency (TF) signature reconstruction exploits the sparsity of nonstationary signals when they are represented in the TF domain. Conventional CS-based approaches, whether the respective linear models involve the ambiguity function or the instantaneous autocorrelation function, do not utilize the continuous structure of the TF signatures. In this paper, a novel approach for sparse nonstationary signal reconstruction was introduced by exploiting the continuous structure of the TF signatures. A patterned prior was used to encourage the structure underlying continuity. It was shown that the proposed technique yields improved performance in the presence of missing data samples due to its capability of preserving the TF signature continuity, discarding anomalies, and effectively suppressing sporadic entries.

## REFERENCES

- [1] P. Flandrin, *Time-Frequency/Time-Scale Analysis*. New York, NY: Academic, 1999.
- [2] B. Boashash, *Time Frequency Signal Analysis and Processing*. New York, NY: Elsevier, 2003.
- [3] M. G. Amin, "Spectral decomposition of time-frequency distribution kernels," *IEEE Trans. Signal Proc.*, vol. 42, no. 5, pp. 1156–1165, 1994.
- [4] Y. Zhang, W. Mu, and M. G. Amin, "Subspace analysis of spatial time-frequency distribution matrices," *IEEE Trans. Signal Proc.*, vol. 49, no. 4, pp. 747–759, 2001.
- [5] M. Hansson, "Multiple window decomposition of time-frequency kernels using a penalty function for suppressed sidelobes," in *Proc. IEEE ICASSP*, (Toulouse, France), May 2006.
- [6] P. Flandrin, M. Amin, S. McLaughlin, and B. Torresani, "Special issue on time-frequency analysis and applications," *IEEE Signal Proc. Mag.*, 2013.
- [7] Y. D. Zhang and M. G. Amin, "Compressive sensing in nonstationary array processing using bilinear transforms," in *Proc. IEEE Sensor Array and Multichannel Signal Proc. Workshop*, (Hoboken, NJ), Jun. 2012.
- [8] Y. D. Zhang, M. G. Amin, and B. Himed, "Reduced interference time-frequency representations and sparse reconstruction of undersampled data," in *Proc. European Signal Proc. Conf.*, (Marrakech, Morocco), Sept. 2013.
- [9] M. G. Amin, Y. D. Zhang, and B. Jekanovic, "Time-frequency signature reconstruction from random observations using multiple measurement vectors," in *Proc. IEEE ICASSP*, (Florence, Italy), May 2014.
- [10] L. Stankovic, S. Stankovic, I. Orovic, and Y. D. Zhang, "Time-frequency analysis of micro-Doppler signals based on compressive sensing," in M. G. Amin (ed.), *Compressive Sensing for Urban Radars*, CRC Press, 2014.
- [11] E. Candes and M. Wakin, "An introduction to compressive sampling," *IEEE Signal Proc. Mag.*, vol. 25, no. 2, pp. 21–30, 2008.
- [12] D. L. Donoho, "Compressed sensing," *IEEE Trans. Info. Theory*, vol. 52, no. 4, pp. 1289–1306, 2006.
- [13] M. G. Amin and W. J. Williams, "High spectral resolution time-frequency distribution kernels," *IEEE Trans. Signal Proc.*, vol. 46, no. 10, pp. 2796–2804, 1998.
- [14] B. Barkat and B. Boashash, "A high-resolution quadratic time-frequency distribution for multicomponent signals analysis," *IEEE Trans. Signal Proc.*, vol. 49, no. 10, pp. 2232–2239, 2001.
- [15] P. Flandrin and P. Borgnat, "Time-frequency energy distributions meet compressed sensing," *IEEE Trans. Signal Proc.*, vol. 58, no. 6, pp. 2974–2982, 2010.
- [16] J. A. Tropp and A. C. Gilbert, "Signal recovery from partial information via orthogonal matching pursuit," *IEEE Trans. Info. Theory*, vol. 53, no. 12, pp. 4655–4666, 2007.
- [17] L. Yu, H. Sun, J. P. Barbot, and G. Zheng, "Bayesian compressive sensing for cluster structured sparse signals," *Signal Proc.*, vol. 92, no. 1, pp. 259–269, 2012.
- [18] L. Wang, L. Zhao, G. Bi, C. Wan, and L. Yang, "Enhanced ISAR imaging by exploiting the continuity of the target scene," *IEEE Trans. Geosci. Remote Sens.*, vol. 52, no. 9, pp. 5736–5750, 2014.
- [19] D. L. Jones and R. G. Baraniuk, "An adaptive optimal-kernel time-frequency representation," *IEEE Trans. Signal Proc.*, vol. 43, no. 10, pp. 2361–2371, 1995.
- [20] B. Jekanovic, M. G. Amin, Y. D. Zhang, and F. Ahmad, "Adaptive time-frequency kernel design for sparse joint-variable signal representations," in *Proc. European Signal Proc. Conf.*, (Lisbon, Portugal), Sept. 2014.
- [21] S. S. Chen, D. L. Donoho, and M. A. Saunders, "Atomic decomposition by basis pursuit," *SIAM Review*, vol. 43, no. 1, pp. 129–159, 2001.
- [22] S. Ji, Y. Xue, and L. Carin, "Bayesian compressive sensing," *IEEE Trans. Signal Proc.*, vol. 56, no. 6, pp. 2346–2356, 2008.
- [23] M. E. Tipping, "Sparse Bayesian shrinkage and selection learning and the relevance vector machine," *J. Machine Learning Research*, vol. 1, no. 9, pp. 211–244, 2001.
- [24] Q. Wu, Y. D. Zhang, M. G. Amin, and B. Himed, "Complex multitask Bayesian compressive sensing," in *Proc. IEEE ICASSP*, (Florence, Italy), May 2014.
- [25] Q. Wu, Y. D. Zhang, M. G. Amin, and B. Himed, "Multi-static passive radar SAR imaging based on Bayesian compressive sensing," in *Proc. SPIE Compressive Sensing Conf.*, (Baltimore, MD), May 2014.
- [26] L. Yu, J. P. Barbot, G. Zheng, and H. Sun, "Compressive sensing for cluster structured sparse signals: Variational Bayes approach," Technical Report, 2011. Available at [http://hal.archives-ouvertes.fr/docs/00/57/39/53/PDF/class\\_vb.pdf](http://hal.archives-ouvertes.fr/docs/00/57/39/53/PDF/class_vb.pdf).